MNRAS **000**, 1–13 (2016) Preprint 17 March 2017 Compiled using MNRAS LATEX style file v3.0

Radiation and supernovae feedback during the epoch of reionization with EMMA

Nicolas Deparis[1]★, Dominique Aubert[1], Pierre Ocvirk[1] and Nicolas Gillet[2]
[1] *Observatoire Astronomique de Strasbourg, CNRS UMR 7550, Universite de Strasbourg, Strasbourg,France*
[2] *Scuola Normale Superiore, Piazza dei Cavalieri 7, I-56126 Pisa, PI, Italy*

Accepted XXX. Received YYY; in original form ZZZ

ABSTRACT

We explore the link between star formation, ionizing sources and supernovae feedback during the epoch of reionization using `EMMA`, a radiative-hydrodynamics (RHD) code with adaptive mesh refinement (AMR). We present a new supernovae feedback model based on kinetic energy injection and constrained by the AMR structure of `EMMA`. We compare this model to simple thermal injection scheme and we show that this model is able to regulate star formation on a wide range of halo masses. We compute the average velocity of galactic winds around halos and we show that our feedback model is able to efficiently generate galactic outflows for halos with masses between $10^8 M_\odot$ and $10^{11} M_\odot$. We also observe outflows due to photo-evaporation by radiative feedback for halos less massive than $10^9 \mathrm{M}_\odot$. We then investigate the influence of the various feedbacks on the reionization process and show that even in the presence of a strong regulation of star formation, the different feedback mechanisms do not impact strongly the simulated reionization history.

Key words: cosmology: dark ages, reionization, first stars - methods: numerical

1 INTRODUCTION

Stellar feedback is a crucial ingredient in the process of galaxy formation. By changing the state of the inter-stellar medium (ISM), stellar feedback introduces a highly nonlinear coupling between the accretion and outflow of gas material in dark matter haloes which is regulating the star formation process in galaxies. Supernovae explode inside star forming regions and blow away the gas that is needed for the future generation of stars to form. Therefore, the more efficient is the star formation process, the more efficient is the feedback and the less efficient is the subsequent star formation process. These effects are especially important during the epoch of reionization when the star formation process is beginning. Understanding the star formation process is therefore crucial during this period in order to correctly follow the build-up of the first generation of ionizing sources.

Supernova feedback was introduced in cosmological simulations mainly for two reasons. First it has been implemented to compensate the overcooling problem which is the fact that the accretion rate of baryons onto dark matter halos in simulation is too high compared to observations. Secondly, supernova feedback was studied to reproduce observed galactic outflows (Veilleux et al. 2005) that have been found to be hard to observe in simulations. Even if supernova feedback is extensively investigated for nearly two decades, its numerical implications are still unclear. The main difficulty is the underlying multi-scale problem where supernova explosion occur at sub-parsec scale while creating gas outflow at scales up to several hundreds of kilo-parsecs.

This is especially hard to tackle in simulations of the reionization process where we ideally want to simulate a very large volume to correctly sample the cosmic variance with the correct abundance of voids and the rare density peaks of the cosmic web. (Iliev et al. 2014) have indeed shown that a volume of 50-100 cMpc is needed to correctly follow the reionization process. Considering such volumes and the actual computation facilities, simulations are still way far to resolve the formation and evolution of individual stars. This is why simulations of these sizes are relying on subgrid modelling for the stellar counterpart.

Different kinds of subgrid modelling have been developped for the supernova feedback with different levels of complexity depending of the spatial resolution of the simulations (Katz 1992; Navarro & White 1993; Springel & Hernquist 2003; Stinson et al. 2006; Dubois & Teyssier 2008; Dalla Vecchia & Schaye 2012).

A few projects have been undertaken to compare the

★ E-mail: nicolas.deparis@astro.unistra.fr

feedback implementations (Kimm et al. 2015; Rosdahl et al. 2016), but there is still no consensus about the right way to deal with it in simulation.

In this work, we focus on the reionization process and we consider that stars in star-forming galaxies are the main emitters of ionizing photons. It has been shown recently that accreting black holes in Active Galactic Nuclei (AGNs) could contribute significantly to the UV photon budget (Giallongo et al. 2015; Haardt & Madau 2012; Chardin et al. 2017; D'Aloisio et al. 2016) However, star-forming galaxies are still the main candidates (Bouwens et al. 2015b). even if it is still unclear how UV radiation can escape the hosting dark matter haloes. Indeed, the way photons propagate through the gas is highly dependent to the local density which depends on the stellar feedback. Therefore, there is a direct link between star formation, stellar feedback and ionizing sources during the reionization process. Understanding where and how stars form is primordial to understand which radiative sources dominate the photon budget.

We introduce the cosmological code `EMMA` in Sec 2.1 as well as our implementation of our star formation and evolution model in Sec. 2.2. An important part of this evolution model is the supernovae feedback scheme, so we present two implementations of supernovae feedback: a classic direct thermal injection described in Sec. 2.3.1 and an original kinetic model constrained by the AMR oct-tree structure of `EMMA` presented in Sec. 2.3.2. We introduce the direct thermal injection implementation for comparison purpose only, as we already know that it will suffer of high radiative losses (Katz 1992), this is the reason why more complex schemes like kinetic feedback was developed. We quantify the influence of the choice of supernovae model on star formation using a set of global variables like the star formation history (SFH) or ionization history, and conclude that our kinetic model is able to efficiently regulate star formation at the cosmic scale. During this test we observe that the energy injection scheme change the SFH, and that even with different SFH, the ionization histories do not seam to be affected. We look at the influence of our main free parameters of our model, which is the feedback and star formation efficiencies. We then consider star formation function of halo masses, show that the regulation of star formation is linked with a decrease in the halo's baryon fraction. We link this decreased in baryon fraction to hydrodynamical flows around halo, and show that feedback push baryons out of halo by generating galactic winds. We also observe during this analyze, the photo-evaporation of baryon due to radiative feedback. We conclude that the regulation of star formation append due to a lack of star forming material due to its expulsion by supernovae feedback.

Our main interrogation is what are the mains physical processes who can explain a significant decrease in the photon budget, without impacting the reionization history. We conclude that either the change in the distribution of baryon by feedback plays an important role in the regulation of the escape fraction of photons to the IGM, or either supernovae do not impact halo responsible to the cosmic SFH.

2 METHODOLOGY

In this section we describe our modelling of cosmic reionization with the `EMMA` code. We will take particular care to explain our supernova feedback implementation as well as our star formation prescription. We will finaly give our initial set-up and the description of the different simulations studied in this paper.

2.1 Code description

We perform cosmological radiative hydrodynamic simulation with the `EMMA` (Aubert et al. 2015) code, an Adaptive Mesh Refinement (AMR) based code designed to studying the Epoch of Reionization (EoR). The code follows the evolution of three distinct physics: the colisionless Dark Matter (DM) dynamics, the gas dynamics, and the radiative transfer of ionizing photons with all the different modules self-consistently coupled to each other.

`EMMA` uses a fully treated three AMR description (Khokhlov 1998). The collisionless dynamics – dark matter and stars – use a particle based representation (Hockney & Eastwood 1981). The gravitational density field is determined from the particle using a Cloud In Cell (CIC) projection. The Poisson equation is solved using a multigrid relaxation method on the base level, and a Gauss-Seidel relaxation on the sub levels. The hydrodynamics solver is based on a piecewise linear method a la MUSCL-Hancock driven by HLLC Riemann solvers (Toro 1997). Finally, the radiation propagation is solved using a moment-based description, with the M1 closure approximation (Aubert & Teyssier 2008; Aubert & Teyssier 2010).

2.2 Star formation

In the two following subsections, we introduce our star formation and feedback models, as well as their free parameters. We are only focusing here on the general model implementation and all details about free parameters values used in this study can be found in Sec. 2.4.

To flag star forming regions, we use a simple overdensity criterion δ . For every cells above this threshold, we compute the Star Formation Rate (SFR) :

$$\dot{\rho} = \epsilon \frac{\rho_g}{t_{\rm ff}}, \tag{1}$$

with ϵ an efficiency parameter, ρ_g the local gas density and $t_{\rm ff}$ a local free fall time expressed as :

$$t_{\rm ff} = \sqrt{\frac{3\pi}{32 G \rho_g}}, \tag{2}$$

This leads to $\dot{\rho} \propto \rho_g^{1.5}$ close to the observational Schmidt-Kennicutt law (Kennicutt 1998).

Based on this SFR, we express the total mass to convert from gas to stars depending on the volume of the current cell dv and the current timestep dt:

$$M_\star = \dot{\rho} \cdot dv \cdot dt. \tag{3}$$

We then follow Rasera & Teyssier (2006), and define a stellar quantum mass of $m_\star$. Using $n_\star = \frac{M_\star}{m_\star}$, we compute an

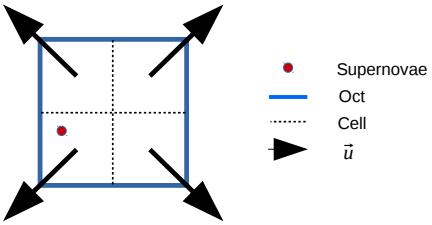

Figure 1. Kinetic energy injection scheme. No matter where the particle is in the oct, the explosion occurs radially from the center of the oct.

average number $n_\star$ of stellar particles to create. We finally draw the final number of particles $N_\star$ to inject in a Poisson law of parameter $n_\star$.

The star particles that are created are placed randomly in the cell volume with a velocity corresponding to the local gas velocity plus a component with a random direction and a random amplitude bound by the local sound speed. During the process of star formation, the mass conservation is obviously respected.

2.3 Supernovae feedback

In this section, we discuss how we implement two different feedback methods. For both methods we dispose of a given amount of energy E_{SN} to inject in the hydrodynamical solver changing either internal or kinetic energy of the gas around the explosion.

2.3.1 Thermal feedback implementation

The thermal feedback model is the simplest way to inject energy. Such an implementation consists in the energy injection by modifying the local pressure:

$$\Delta P = \frac{E_{SN}}{dV}(\gamma - 1), \tag{4}$$

where dV is the cell volume and γ the adiabatic index.

Once the energy injection has been done, a fraction f_r of the stellar particle mass is returned and put back into the cell. The total mass return is $m_r = f_r \cdot m_\star$.

We use this feedback for comparison purpose only.

2.3.2 Kinetic feedback implementation

Historically, kinetic feedback was developed after it has been shown that thermal feedback suffers from high radiative losses and is inefficient to generate galactic outflows (Navarro & White 1993). Kinetic feedback consists into modifying the velocity of the gas in cells around the explosion instead of its internal energy. Its main advantage is that it override the conversion of heat into movement, highly inefficient when cooling processes are allowed. But its main inconvenient its that it leads to a lose of resolution. Indeed, when a thermal scheme can heat an unique cell, kinetic need to change the properties of the gas in a bigger number of cells to result in a spherical explosion. Moreover, the bigger the number of cells is, the more spherical the resulted blast wave will be. On an AMR grid, finding neighbor has a cost and the counter part of a rounder explosion is that the numerical cost of finding the considered cells will quickly rise. Furthermore, due to the parallel nature of computations in `EMMA`, if an explosion occurs at an edge of a processor domain, distributing the explosion along the cells will result in costly communications. In our case, we limit the number of cells in which the explosion occurs to 8 and, using the AMR octtree structure of `EMMA`, theses eight cells have to share the same parent oct. This almost reduce to zero the cost of the neighbor search, and totally avoid communication between processors Moreover, this also allows us to be sure that cells where the feedback is computed are all at the same level of resolution, which ensure us a certain homogeneity in the explosion. A schematic view of our injection scheme is given in Fig. 1.

We divide the total available energy, uniformly into theses eight cells, so each cell receives,

$$e_{SN} = E_{SN}/8. \tag{5}$$

Finally, e_{SN} is used to change the gas velocity of each cell,

$$\Delta\overrightarrow{v_{gas}} = \sqrt{\frac{2e_{SN}}{\rho_g . dV}}\,\overrightarrow{u}, \tag{6}$$

where $\overrightarrow{u}$ is the unit vector pointing radially from the center of the oct. The mass is returned in the same way as for the thermal feedback except that each cell now receives one-eight of the total available mass.

Name	ϵ_{SF}	f_{esc}	Supernovae	ϵ_{SN}
noFEED	0.5%	0	-	0
noSN/$\epsilon_{SN}=0$	0.5%	0.4	-	0
$\epsilon_{SN}=0.1$	0.5%	0.4	Kinetic	0.1
$\epsilon_{SN}=0.5$	0.5%	0.4	Kinetic	0.5
$\epsilon_{SN}=1$	0.5%	0.4	Kinetic	1
Thermal	0.5%	0.4	Thermal	1
Kinetic/SF05	0.5%	0.4	Kinetic	1
SF2	2%	0.4	Kinetic	1
SF10	10%	0.4	Kinetic	1

Table 1. Simulations features investigated in this study. The parameters are: the identification run name, the star formation efficiency ϵ_{SF}, photon escape fraction f_{esc}, type of supernovae feedback method and the efficiency of supernovae feedback ϵ_{SN}. All theses runs share the same initial conditions described in Sec. 2.4.

2.4 Calibration and initial conditions

In the following we consider a $8/h$ comoving Mega parsec (cMpc) cube boxes (≈ 12cMpc)^3, resolved with 256^3 dark matter particles. This leads to a DM mass resolution of $3.4 \cdot 10^6 M_\odot$, and a spatial resolution of 46ckpc on the coarse grid. Initial Condition (IC) were generated with MUSIC (Hahn & Abel 2011) with a Planck Cosmology (Planck Collaboration et al. (2015) : $\Omega_m = 0.3175$, $\Omega_v = 0.6825$, $\Omega_b = 0.0490$, $H_0 = 67.11$, $\sigma_8 = 0.830$. Simulation starts at redshift $z = 150$. The grid is refined according to a semi-Lagrangian scheme and the refinement is not allowed if the

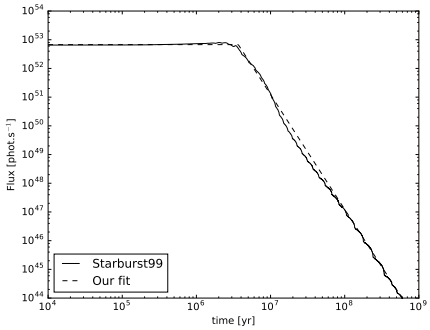

Figure 2. Our ionizing emissivity model presents two phases, a constant emissivity one, and a decreasing one. The transition between theses two phases define the radiative lifetime $t_{\rm life}$.

spatial resolution of the newly formed cells is under 500pc. We use a reduced speed of light of 10% of the real one, coupled with the Coarse Radiative Transport Approximation (CRTA) scheme implemented in the `EMMA` code (see Aubert et al. (2015)).

We use a star formation over-density threshold of $\delta = 50$ and star formation efficiency parameter $\epsilon_{SF} = 0.5\%$. Our model for the ionizing emissivity of the star particles is calibrated using Starburst99 (Leitherer et al. 1999). Because our resolution does not allow to track real individual star particles, we consider each star particle represent a stellar population of $7.2 \cdot 10^4 M_\odot$ with a Top-Heavy Initial Mass Function (IMF) integrated from $0.1 M_\odot$ to $100 M_\odot$ and with a constant metallicity of $Z = 0.001$. Since we are only considering hydrogen reionization, the Starburst99 spectrum is integrated on the energy range from 13.6ev to infinity corresponding to the ionizing spectrum of neutral hydrogen. We get the ionizing emissivity function by doing this integration for all star ages of our population. The ionizing emissivity presents two regimes. First a constant emissivity as a function of time and second a fast emissivity drop (See Fig. 2). During the constant emissivity phase, sources emit $S_0 = 1.55.10^{17}$ phot.sec^{-1}.kg^{-1}. We consider the radiative lifetime $t_{\rm life}$ of sources to be at the transition of theses two regimes: $t_{\rm life} = 3.67.10^6$Myr. After t_{life}, the sources still radiate with a number of photons that is a decreasing power law as a function of time ($S_{(t>t_{\rm life})} \propto t^{-4}$). The calculations are done using a monochromatic photons with a mean energy of $< h\nu >= 23.42$ eV, an energy weighted cross section of $\sigma_e = 2.35.10^{-22}$ m^2 and a number weighted cross section of $\sigma_i = 1.82.10^{-22}$ m^2.

Supernova feedback model are also calibrated using Starburst99 as it gives us access to the temporal evolution of the amount of mass and energy returned in the medium by the considered stellar population. We choose to inject the totality of the available energy instantaneously after a time $t_{\rm lifeSN}$ which is defined as the time where 50% of all the energy from Starburst99 should be released. We use the total amount of energy released by winds and supernovae during the whole lifetime of the population. The quantity of energy injected in our model is regulated by an efficiency parameter ϵ_{SN}. In our model, we also return a mass fraction f_r of the total particle mass when a supernova explodes. All the mass is released instantaneously at the same instant as the energy. In practice, our model parameters are: a life time of $t_{\rm lifeSN} = 17.7$ Myr, a total available energy of $E_{SN} = 2.47 \cdot 10^{42}$J.M$_\odot^{-1}$ and a mass return fraction of $f_r = 52.6\%$.

All runs share the same initial conditions. The only difference between all the different runs is the feedback method. Tab. 1 present a summary of the different runs performed in this study. Our reference run is obtained using a two steps calibration protocol. We run a first simulation without any feedback to calibrate the star formation history on observational constraints from Bouwens et al. (2015a). Based on this SFH, we run a second simulation with radiative feedback to calibrate stars emissivity (via the f_{esc} parameter) to fit observational constraints from Fan et al. (2006).

3 TEMPERATURE AND DENSITY FIELDS AROUND THE MOST MASSIVE HALO

Our first diagnostic is purely qualitative and consists at looking at the density and temperature fields around a specific halo. We choose the most massive halo in the *noSN* simulation, which has a mass of M= $1.10 \cdot 10^{11}$M$_\odot$, corresponding to a R_{200} radius of 21kpc at redshift $z = 6$. Fig. 3 represents a $214 \times 214 \times 6.5$ kpc slice at redshift $z = 6$, centered on this halo, for simulation without supernovae feedback (first row), with direct thermal injection (middle row) and with our kinetic model (bottom row).

Compared to the one of the *noSN* run, the density map of the *thermal* run is a bit more fluffy around mains overdensities (in red). There is apparition of thin concentric overdense region (in white) around some halos, for example in the top right filament or around the further over-density in the bottom right filament. These shells are due to the shock of the outflowing gas on the IGM. On the temperature map, the main halo is able to generate a bigger hot bubble with thermal feedback than without, but different is also clear on the bottom right filament where the hot bubble were almost non present in the run without feedback.

If we now look at the *kinetic* run, we clearly see a more important impact on both fields than with the thermal injection method. Outflows are significantly stronger and there is apparition of shock shells around the main halo with a radius of several R_{200} and a density of about ten time the average density (in white). Furthermore, the hot region is also wider and correspond to the inner shock radius defined by the shells in the density map.

The hot region ($T > 10^5$K) in a $5 \cdot R_{200}$ box around the halo represent a volume fraction of $f_V = 0.3\%$ and a total mass of $M_{hot} = 1.9 \cdot 10^9 M_\odot$ for the *noSN* run, compared to $f_V = 1.0\%$ and $M_{hot} = 4.2 \cdot 10^9 M_\odot$ for the thermal run and $f_V = 2.7\%$ and $M_{hot} = 7.3 \cdot 10^9 M_\odot$ for the kinetic run. Around this specific halo, the kinetic feedback can heat 2.7 times more volume and 1.7 time more mass of gas.

4 STAR FORMATION AND IONIZATION HISTORIES

Cosmological star formation history is the first observable we try to fit in reionization simulations. It offers a good global diagnostic of the simulation state, as it considers the whole

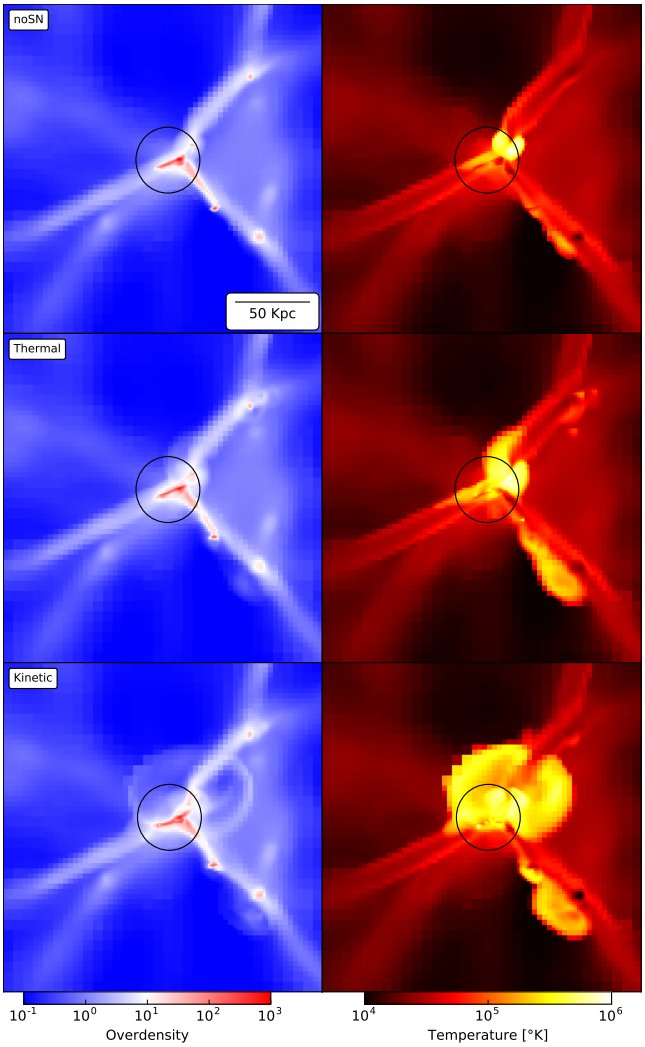

Figure 3. Most massive halo of the simulation (M≈ 10^{11}M$_{\odot}$) at redshift $z = 6$. Average over a 7kpc thick slice of overdensity (left) and temperature (right), without feedback (top), with thermal feedback (middle) and with kinetic feedback (bottom). The black circle represent the R_{200} = 21kpc. With the same quantity of energy injected, kinetic feedback can generate much bigger hot bubble ($T > 10^5 K$) around halo than thermal one.

simulated volume and could be easily compared to observational constraints. Furthermore, supernovae feedback was introduced in numerical simulations with the primary goal to regulate star formation by diluting baryon over-densities. Feedback should not be neutral on the cosmic SFH and ideally, all energy injection methods should lead to the same response of the simulation.

The second observable we want to constraint is the cosmic ionization fraction history. We expect a direct link between ionization history and the SFH as ionizing photons are mainly emitted by newly formed stars (see our ionizing emissivity model on Fig. 2) but we will see that this link is not as direct as expected.

In this section we look at how a change in the energy injection model, in the star formation efficiency or in the amount of energy injected, influence theses two observables.

4.1 Influence of the energy injection method on integrated observables

We want to explore the influence of the energy injection method on the regulation of star formation, so we compare three simulations, one without feedback, one with thermal feedback , and one with kinetic feedback. Theses three simulations are run with radiative processes and with the same initial setup. In addition to theses three simulations, we use a reference simulation without radiative sources to measure the influence of radiative transfer feedback.

We observe on Fig 4a that, with the same quantity of energy injected, the injection method significantly changes the cosmic SFH. The *Thermal* run (in red) gets a SFR slightly lower than the *noSN* run (in black), and as expected is not as efficient as the kinetic model to regulate star formation. With the same amount of injected energy by unit mass of formed stars, at redshift $z = 6$ the SFR of the *Kinetic* run (in green) is lowered by a factor ≈ 3, compared to the *noSN* run (in black).

For each methods, the feedback induces a decrease in the SFR, so the total number of emitted photons is not the same between simulations. But we observe on Fig. 4b, that in theses three simulations the reionization occurs almost at the same redshift. The small delay between their reionization redshift is in accordance with their SFH, ie lower SFH leads to a later reionization. But this delay is smaller than what we could expect just from the lowering of the photon budget. Indeed, at redshift $z = 8$, the kinetic feedback decreases the SFR by a factor ≈ 3 and thus the number of emitted photon is also lowered by approximately the same factor. At redshift $z = 8$, less than half the volume is ionized, but the ionization rate – the slope of the ionization history curve – is not affected by the lowering of emissivity due to feedback.

This diminution of the number of emitted photon without changing ionization history is our main interrogation here, and in the following, we focus on exploring different effects that can lead to this observation. But before, we push a bit further the interpretation of measures presented on Fig.4.

If we only focus on radiative feedback effects, by comparing the differences between the *noFEED* run and the *noSN* run, we can quantify the influence of radiation on the SFH. On Fig. 4a we observe that the *noFEED* run (in black dot) get almost the same SFH than the *noSN* run (in black). It means that radiation get a small feedback on halos responsible of the global SFH. The fact that radiation gets a negligible impact on the cosmic star formations history validates our two steps calibration protocol (Sec. 2.4). Obviously, the *noFEED* run (black dotted curve on Fig. 4b) do not reionize and stay with an ionization fraction only governed by collisional ionization.

Star formation processes are dependent of the gas density, which is itself strongly dependent of the resolution. On the Fig. 4a, the bump in the SFH at redshift $z \approx 10$ is due to the triggering of the last refinement level $L_{max} = 11$ at redshift $Z = 10.6$.

We conclude from this diagnostics, that our kinetic feedback implementation is able to regulate cosmic star formation rate and that independently of the energy injection method, reionization occurs at the same time.

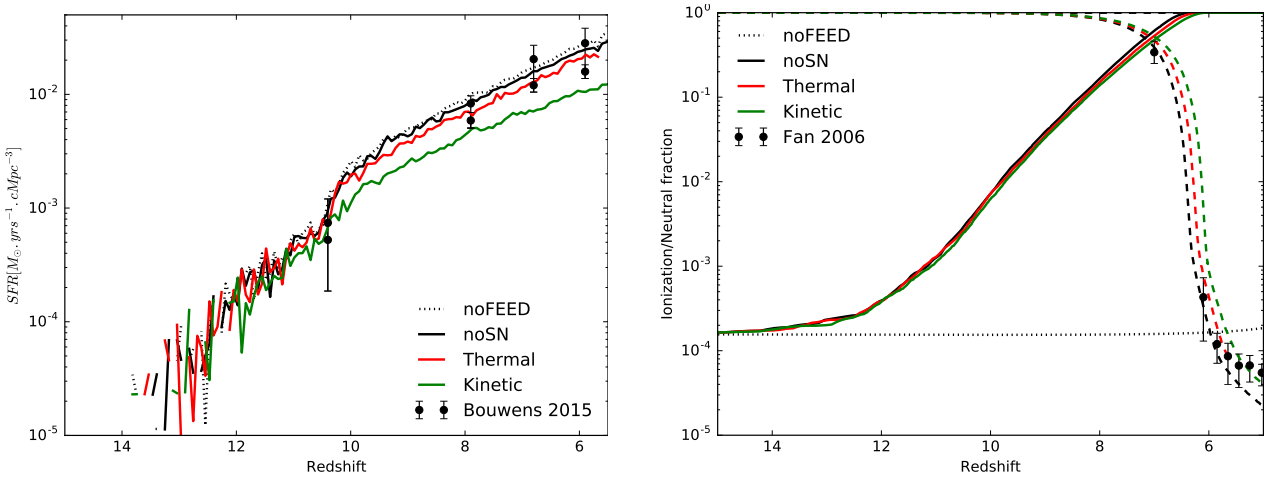

(a) (b)

Figure 4. (a) Cosmic star formation histories and (b) volume weighted ionization (solid lines) and neutral (dashed lines) fraction function of redshift for different feedback method. The introduction of radiation get a small impact on the cosmic SFH. The kinetic method get a significantly stronger effect on the SFH than the thermal model. Reionization occurs almost at the same redshift independently of feedback scheme.

4.2 Influence of the supernovae feedback efficiency parameter

The main free parameter of our energy injection model is its subgrid efficiency ϵ_{SN}. Its will regulate the quantity of energy effectively injected in the gas at the cell scale's. Our stellar population model, returns the amount of energy released in the medium from a point of view of stars. The ϵ_{SN} parameter is a way to regroup different physics like turbulence or infrared radiative losses acting at scales not resolved in our simulation. In all case we know that there is losses during the explosion process and that ϵ_{SN} has great chances to be lower than the unity.

In this section, we run four simulations with different feedback efficiencies ($\epsilon_{SN} = 0.0; 0.1; 0.5; 1.0$), and look at how cosmic star formation and ionization histories are impacted by a change in the amount of energy injected, results are presented on Fig. 5. As we expected, the more we inject energy, the more we reduce the global SFR (Fig. 5a). Furthermore, we observe the same behavior as the previous section: the regulation of stars formation by supernovae feedback do not significantly change the reionization history (Fig. 5b).

We note that the run with the $\epsilon_{SN} = 0.1$ efficiency shows a comparable SFH to the one of the *Thermal* run (red curves in both Fig. 4a and Fig. 5a). We estimate that the thermal feedback scheme suffer of around 90% of radiative losses compared to the kinetic scheme.

This test does not allows us to conclude about the final quantity of energy to inject, but we observe that if we inject the totality of the energy available from Starburst99 model (the $\epsilon_{SN} = 1$ run), the SFR is decreased by a factor ≈ 3 at redshift $z = 6$, which is enough to go out of observational constraints. In the next section we try to get back into the constrains by increasing the star formation efficiency .

4.3 Influence of the star formation efficiency parameter

We now want to explore the degeneracy between the star formation efficiency parameter ϵ_{SF} and the supernovae feedback. Indeed, increasing star formation efficiency leads to transforming more gas into stars, and thus increasing the amount of feedback, but increasing the feedback results in decreasing the star formation rate. It is not clear how the simulation will respond to a change in the star formation efficiency with a given supernovae feedback. In the following, we use the kinetic feedback scheme with an efficiency of $\epsilon_{SN} = 1$ and run three simulations with star formation efficiency of $\epsilon_{SF} = 0.5\%$, $\epsilon_{SF} = 2\%$ and $\epsilon_{SF} = 10\%$. Fig. 6a presents the obtained star formation histories. We observe that increasing star formation efficiency leads to generate first stars at higher redshift and in greater quantity, but that with time the feedback become sufficiently strong to change the shape of the SFH.

At high redshift, the SFH seems to be only regulated by the ϵ_{SF} parameters, the larger ϵ_{SF} is, the more the stars form. Moreover, independently of ϵ_{SF}, the SFH slope tend to be constant in this high z regime. At this time, star formation is almost only regulated by the collapse of structures, and the effect of feedback seems to be negligible when averaged on the whole volume. But with decreasing redshift, the cumulative effect of feedback become stronger, and then the slope significantly changes depending on ϵ_{SF}. With high star formation efficiency ($\epsilon_{SF} = 10\%$, in blue), the amount of injected energy became sufficient to generate a decreasing star formation history. We observe a counter-intuitive effect: increasing star formation efficiency can leads to decrease the star formation rate.

As increasing feedback do not just shift the whole SFH down, but significantly change its shape, we conclude that we cannot fit SFH observation with $\epsilon_{SN} = 1$, even by increasing the star formation efficiency. The feedback efficiency parameter ϵ_{SN} has to be lower than 1 to fit the observations,

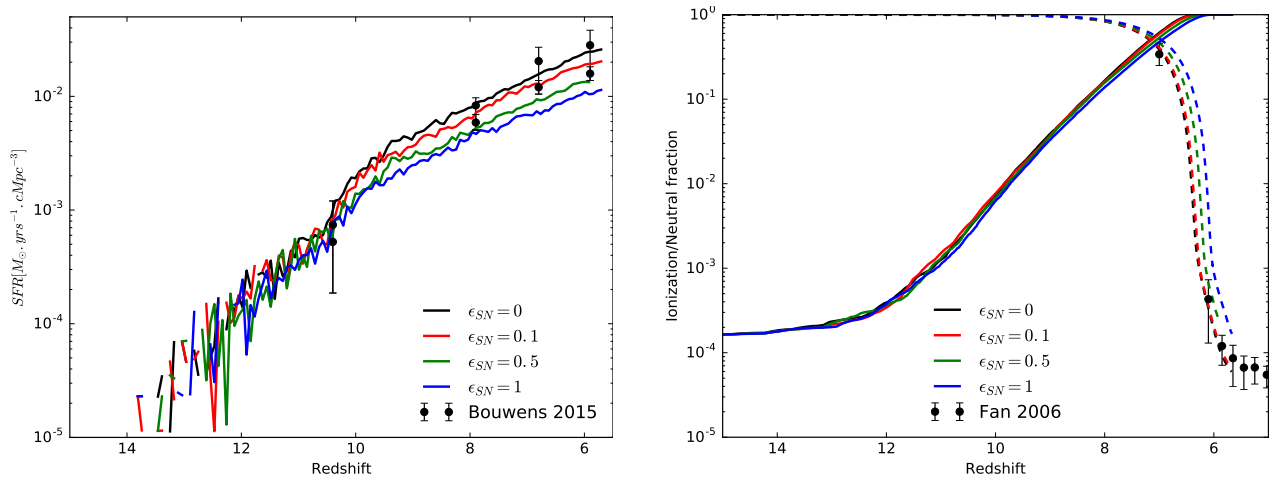

(a) (b)

Figure 5. (a) Cosmic SFH and (b) volume weighted ionization (solid line) and neutral (dashed line) fraction function of feedback efficiency parameter ϵ_{SN} for the kinetic feedback model. The regulation of star formation is directly linked with the quantity of energy injected in the medium. The ionization history is not impacted by the change in the SFH due to supernovae feedback.

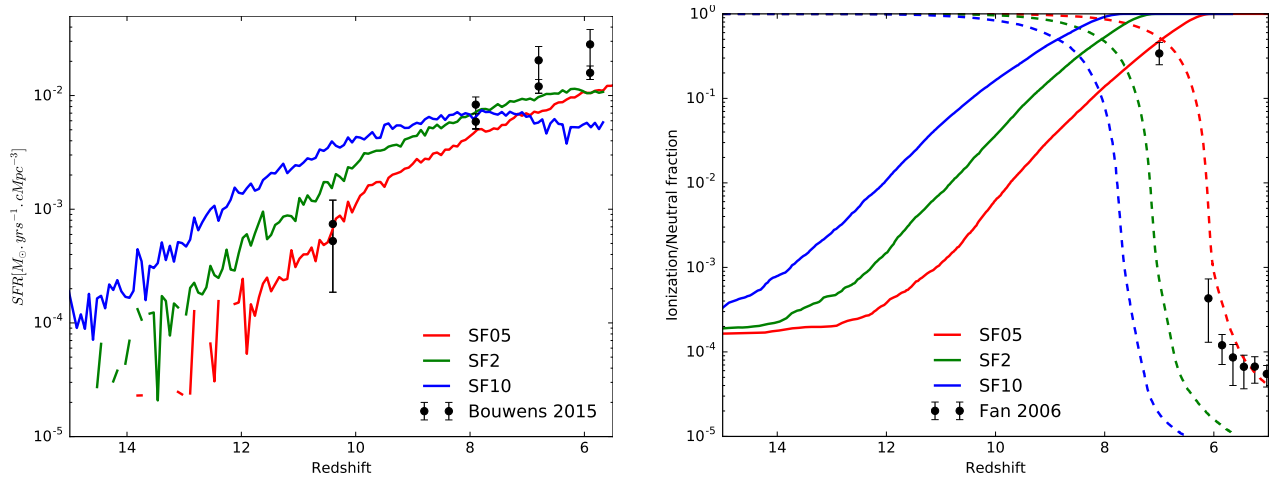

(a) (b)

Figure 6. (a) Star formation and (b) volume weighted ionization histories for different star formation efficiency ϵ_{SN} with high efficiency (ϵ_{SN} = 1) kinetic feedback. Due to feedback, increasing star formation efficiency can lead to lower the SFR.

which is a reasonable assumption, as there are losses in the subgrid scheme (eg radiation or turbulence) that we do not models.

If we now pay attention to the ionization histories (Fig. 6b), we observe a significant change in the reionization redshift. As expected, the more efficient the star formation is, the sooner the reionization happen. As stars appear sooner in the volume with higher star formation efficiency, the medium starts to reionize at higher redshift. But as the feedback needs time to be efficient at regulating the SFR, it also needs time to regulate the ionization rate. There is a small change in the slope of the *SF10* curve (in blue on Fig. 6b) after redshift $z \approx 11$, due to the cut in the SFR. But the effect of feedback do not seems to be sufficient to stop the reionizing processes, at least in the range of parameters we explore, however, it may be possible, if we push the efficiency further, that the SFR cutout will be sufficient to keep the box away from reionizing.

5 HALO MASS DEPENDENCY

5.1 Star formation and baryon fraction

The balance between star formation and feedback, function of halo mass, is not obvious. Indeed, low masses halos ($M < 10^9 M_\odot$) do not form much stars and thus are not exposed to a large amount of feedback, however they do not get a strong gravitational potential to hold their baryon back, so if stellar population form in this light halos, supernovas events can blast a significant part of the gas. On a other side, high masses halos ($M > 10^{10} M_\odot$) host large star formation events and are exposed to strong feedback processes,

but their gravitational potential is much more able to keep their baryon in.

In this section we explore the competition between the accretion of star forming material by gravitational potential and its expulsion by stellar feedback. We focus on the quantification of which class of halos masses see its instantaneous SFR more impacted by feedback, at the end of the reionization at redshift z=6.

Moreover low masses halos ($M < 10^9 M_\odot$) are predominant in number but they get a lower SFR, so they do not host large quantity of UV emitting stars. At the opposite, high masses halos do emit a strong UV field but are far less numerous. What are the respective contributions of each classes of masses on the photons budget and how this budget is influence by feedback?

We compute instantaneous star formation rate for each halos by measuring the total stellar mass appeared within its R_{200} during the last 10Myr :

$$SFR_{10}^{halo} = \frac{\sum M_\star \left(r < R_{200}^{halo}; t < 10\mathrm{Myr}\right)}{10\mathrm{Myr}}. \quad (7)$$

The correlation between the halo mass and its instantaneous SFR is presented on Fig. 7a. In all case, the introduction of feedback leads to a decrease in the SFR and change the slope of this correlation. Radiative and thermal feedback (in red) tend to be more efficient at lowering the SFR for low mass halos ($M < 10^9 M_\odot$) while kinetic feedback (in green) tends to act on heavy halo ($M > 10^{10} M_\odot$).

If we now look at SFR_{bin}, the total contribution of a class of halos masses to the cosmic SFR:

$$SFR_{bin} = \sum_{halo} SFR_{10}^{halo} \left(M_{bin} \leq M^{halo} < M_{bin} + dM\right), \quad (8)$$

presented on Fig. 7b, we see that smallest halos ($M < 10^9 M_\odot$), do not represent a significant fraction of the global SFR at this time, even if they are the most numerous. In return, halos around $10^{10} M_\odot$ are the main contributors of the cosmic SFR at $z = 6$. For the *noFEED* run, the cumulative SFR seems to decrease for halo heavier than $10^{10} M_\odot$, however, it is not clear if it is a statistical effect due to the limited size of the simulation or a physical effect. Independently of the feedback type, halos under $10^9 M_\odot$ are not the main contributors of the SFR and thus of the UV photon budget at $z = 6$. To alter the cosmic SFH, a feedback scheme has to change SFR in the predominant class of halos masses. We see from Fig 7a that kinetic injection is the most efficient to regulate star formation in this range of masses ($M > 10^{10} M_\odot$), and thus the most efficient to regulate the whole cosmic SFR.

If kinetic feedback tends to decrease more the global SFH, it is because it gets impact on halos responsible of the global SFR, while thermal feedback gets a small impact because it acts on halos with a negligible SFR contribution.

We just identified where feedback act, we now focus on why does the feedback change star formation processes. The only field responsible to the SFR is the gas density (see Eq. 1), so an efficient feedback should break over-densities responsible to stars formation. And as these over-densities are located in halos, we expect that the decrease in the halo's SFR is due a diminution of the quantity of baryon belonging to it. We observe that the averaged baryon fraction for

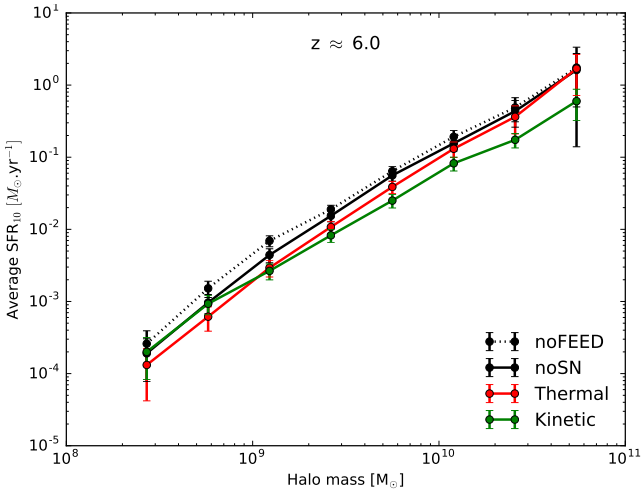

(a)

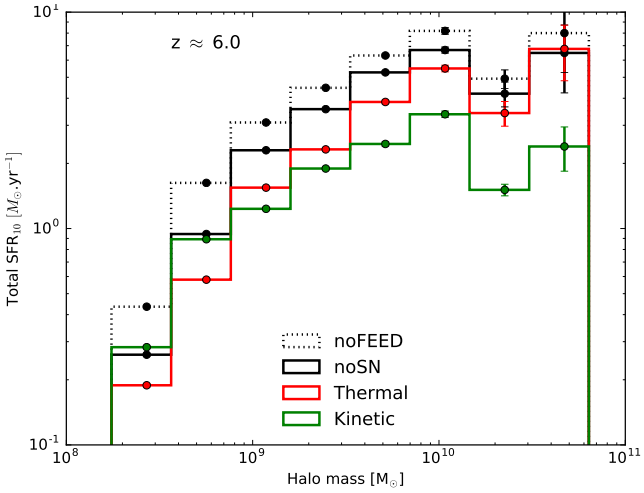

(b)

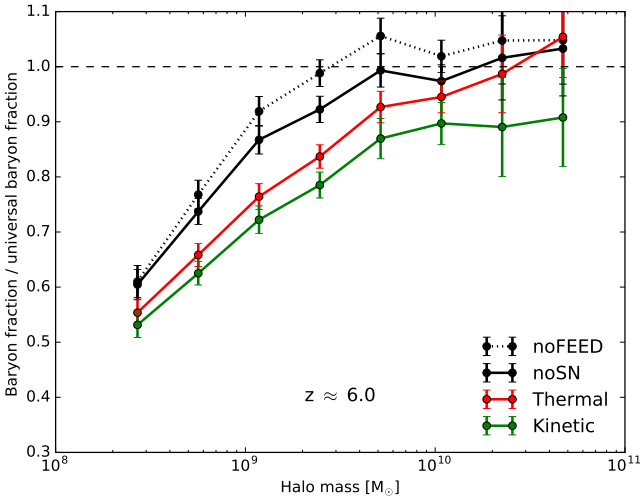

(c)

Figure 7. Star formation rate averaged (a), binned (b) and average baryon fraction (c) by bins of halo mass at redshift z=6 for different feedback methods. Thermal feedback tend to have impact on smallest halos, while kinetic form reduce the SFR on the biggest one. Halo with masses around $10^{10} M_\odot$ are responsible of the major fraction of the global SFR, and thus of the photon budget.

a class of masses (Fig. 7c) is linked to the SFR. For all ranges of masses, the lower the baryon fraction is, the less the SFR is. This is particularly clear for halos with masses over 10^{10}M$_\odot$: the SFR is not impacted by thermal feedback (in red) and the baryon fraction is almost universal, but for kinetic feedback (in green) we observe a diminution of the baryon fraction and therefore of the SFR.

Having more baryons in halos allows more stars formation, but in term of radiative processes, it could also reduce the escape fraction of photons. Stars are born in baryon over-densities, but radiation can be trapped by these over-densities, due to high recombination rate. The role of feedback is to break these blob of gas, limiting star formation but allowing radiation to escape halos more easily. As we shown in Fig. 4, the balance seems to be almost neutral, as feedback effectively regulates star formation but at the same time does not change the reionization redshift. Even if there is less UV sources in the volume, ionized regions grow at the same rate, thus either the escape fraction of photons should be increased by feedback (Kimm & Cen 2014; Trebitsch et al. 2015) or the suppression of star formation acts mostly on halos who are not responsible of the average ionizing state.

5.2 Average R_{200} flow speed

In this section, we investigate the evolution of the average radial velocity of the gas around halos depending on the feedback scheme. To compute these velocities, we draw a virtual sphere around each halo with a given radius and centered on the center of mass of the halo. The resulting velocities are functions of the distance from the halo. Here we arbitrary take the R_{200} as our reference radius.

The general expression for the average radial velocity $\bar{v}$, is:

$$\bar{v} = \frac{\oint \vec{v} \cdot d\vec{s}}{\oint d\vec{s}}, \tag{9}$$

but as each sphere is discretized with 3072 HEALPix points (Górski et al. 2005), the average radial velocity became:

$$\bar{v} = \frac{1}{N} \sum_{i=1}^{N} \vec{v_i} \cdot \vec{r_i}, \tag{10}$$

with N the number of HEALPix points, $\vec{v_i}$ the gas velocity of the nearest cell of point i and the normal vector $\vec{r_i}$ oriented outward. Therefore, positive values stand for outflow and negatives one for inflow. Fig. 8 presents the resulting average velocities as a function of halo masses for the different feedback schemes. Each halo is represented by a dot, with a different color depending if it has stars, young stars or no stars. The upper part of the diagram represents outflows and the lower part represents inflows.

The dashed lines are defined by:

$$v_{lim} = \pm\sqrt{\frac{2GM_{(r<R_{200})}}{R_{200}}}, \tag{11}$$

and represent the free fall velocity limit for the inflowing case, and the escape velocity for the outflowing case.

Without feedback (Fig. 8a) almost all halos are in the negative part of the diagram, they are all accumulating baryons. The correlation between inflow speeds and halo masses is particularly sharp with this run, and at this redshift ($z = 6$). At high redshift the dynamic is still relatively simple as there is no time for complex merger event, and as there is no feedback, the dynamic is mostly governed by gravity and structures are almost all collapsing.

This free fall tendency tends to be an upper limit of the accretion velocity, and only few halos have average inflow velocity with an absolute value over this limit. Also, we note that the velocity dispersion became wider as halos became less massive and there is no major difference between halos with and halos without stars.

With the introduction of radiation (Fig. 8b), there is an increase in the dispersion of velocity values. This increase is more pronounced on halos lighter than $3 \cdot 10^8 M_\odot$ and specially starless ones (light red population) at a point that a part of this population starts to get net outflows (in light blue). The fact that the major part of this population do not have stars, says that theses outflows are not due to internal feedback, and suggest an external effect. Our interpretation is that these light halos are submitted to a UV field created by surrounding halos massive enough to get stars. We are observing the effect of photo-heating by radiative feedback, the gas heated by radiation expands and leaves its host by dilution. It escapes only from halos of low masses because heavier halos get a sufficient potential to hold their baryons.

With an average speed ≈ 0.5km.s^{-1} theses outflows are relatively slow and all velocities are under the escape velocity, so baryon are still gravitationally linked to their host.

There is also a small shift, present for almost all the halos masses range, in inflowing speeds: inflows tend to be slightly slower due to photo-heating.

Radiation generates outflows and slow down the collapse of gas, reducing the quantity of available star forming material by limiting the accretion. Moreover, even if we are not considering molecular hydrogen chemistry in theses runs, UV radiation break H_2 molecules and thus limit the cooling rate (Haiman et al. 1997). So we could expect a double effect of radiative feedback on star formation processes: radiation blocks stars formation by on one side, reducing the accretion by photo-heating and on the other side, keep it away from cooling due to the destruction of molecular hydrogen.

If we now focus on the two runs with supernovae feedback (Fig. 8c and 8d), we clearly see that there is apparition of a new population of halos with outflows and that almost all those halos have stars (dark blue). Those halos are under the influence of an inner effect due to stars, we see here the influence of supernovae feedback pushong the gas out of halos. Supernovae feedback also limit the accretion, the dispersion of inflowing halos with stars (dark red) is significantly increased. This idea is supported by the fact that the distribution of starless halos stay mainly unchanged compared to RT only run (Fig. 8b).

The mean outflow speed is now close to 10km.s^{-1} which is twenty times greater than for the *noSN* run. Some light halos ($M < 10^9 M_\odot$) get average outflow speed over the escape velocity, theses halos are literally blasted by feedback.

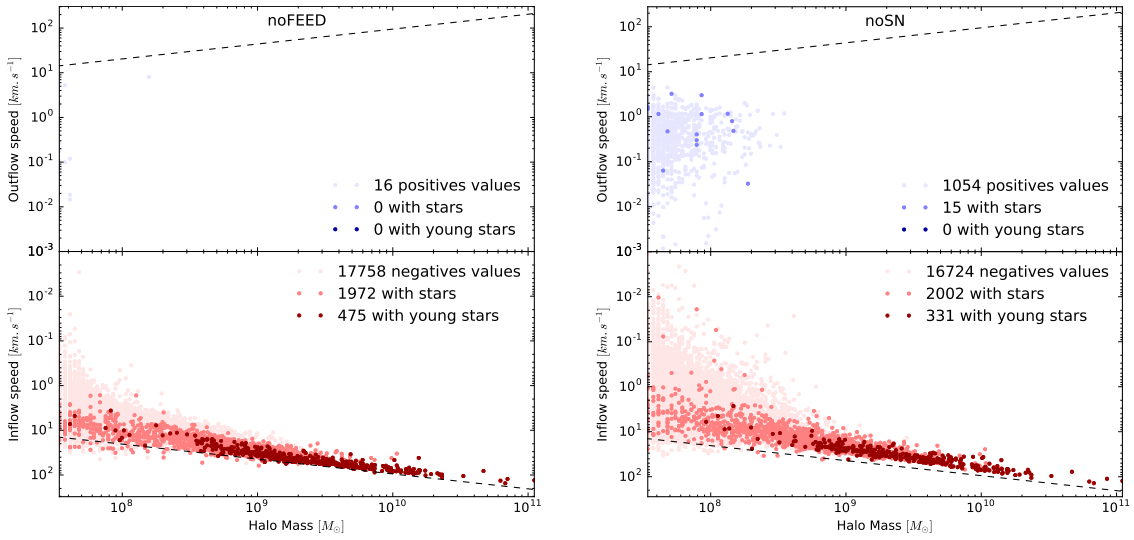

(a) Without feedback

(b) Radiative transfert (RT) only

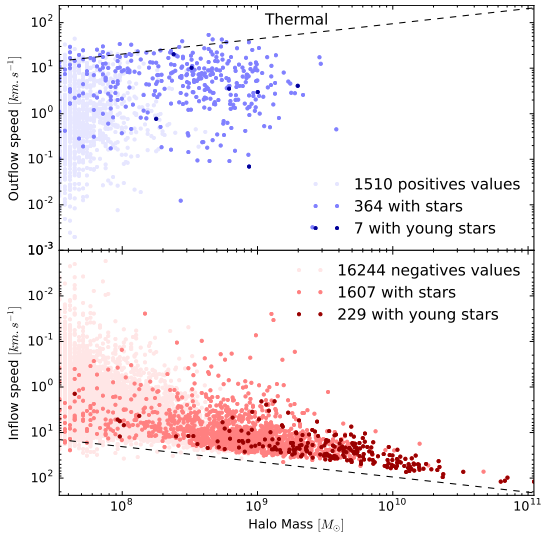

(c) RT + thermal SN

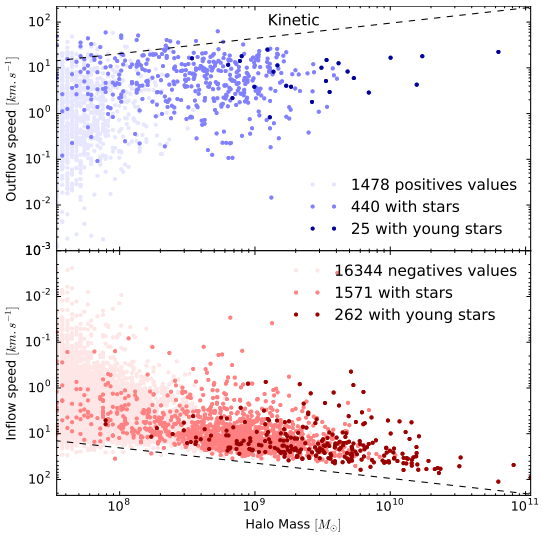

(d) RT + kinetic SN

Figure 8. Average hydrodynamical flow speed at R_{200} function of injection method measured at redshift z=6. Blue dots represent halos with outflow, red with inflow. Light dots represent halos without stars while dark dots are for halos with stars. The dashed line represents ± the escape velocity. Without radiation there is almost no halo with a positive average speed (outflowing matter). The introduction of radiation leads to the apparition of a population of starless low mass halos ($M < 3 \cdot 10^8 M_\odot$) with outflow. Supernovae introduce a population of outflowing halos with stars. Kinetic feedback allows heavier halos to get outflow than thermal feedback.

It seems that the feedback type does not change the maximum outflow speed ($\approx$ 60km.s^{-1}), but only allows bigger halos to get a positive average speed. The most massive halo with outflow in the *noSN* simulation weight $3.5 \cdot 10^8 M_\odot$, $3.6 \cdot 10^9 M_\odot$ in the *thermal* run and $6.3 \cdot 10^{10} M_\odot$ in the *kinetic* run. Outflow velocities can seem low compared to observed ones (between $\approx$ 20 and $\approx$ 2000Km.s^{-1} according to Veilleux et al. (2005)) but we are considering averaged values, taken individually, velocities can be as high as 600km.s^{-1} at the R_{200} level, and 1500km.s^{-1} in a cell where the explosion occurs, which is in the typical range of observed velocities.

5.3 Influence of supernovae feedback scheme on halo emissivity

In this section we want to quantify how the emissivity of halo change, function of the supernovae energy injection scheme.

Due to the moment based treatment of radiation, we can use a procedure similar to our hydrodynamical analysis (Sec 5.2) to compute F_{200}, the halo emissivity at R_{200}, by integrating the radiative flux field $\vec{F}_{rad}$ for each halo:

$$F_{200}^{halo} = \oint_{R_{200}^{halo}} \vec{F}_{rad} \cdot d\vec{s}. \quad (12)$$

Also, in a similar way that in Eq. 8, we can sum these

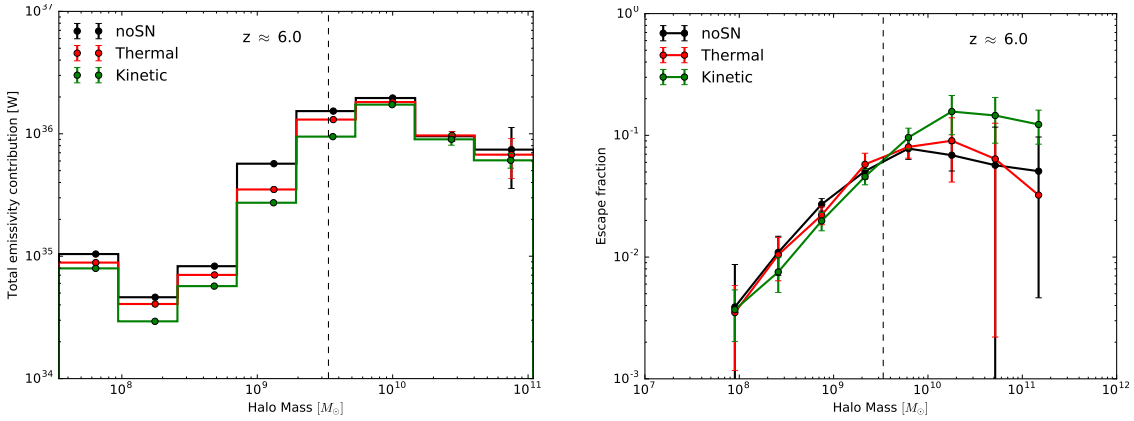

(a) Total emissivity (b) Estimated average escape fraction

Figure 9. Total emissivity contribution (a) and escape fraction (b) as a function of halo mass, for different feedback scheme. All measures are done at redshift z=6. The dashed line represent the halo mass equivalent to our radiative resolution limit. For heavy ($M > 10^{10} M_\odot$), radiatively well resolved halos, emissivity stay almost identical independently of the feedback scheme. We observe a significant increase in the escape fraction of heavy halos with the kinetic scheme.

F_{200} by masses bins, and estimate the photon budget distribution:

$$F_{bin} = \sum_{halo} F_{200}^{halo} \left(M_{bin} \leq M^{halo} < M_{bin} + dM \right). \quad (13)$$

Fig. 9a presents F_{bin}, the total emissivity of halos in a range of masses for our three feedback schemes.

The first observation is that there are two regimes in this diagram, most massive halos represent the biggest part of the emissivity while lightest ones are about ten times fainter. Also, it seems that the total emissivity of heavier halos tend to decrease with the halo mass, however it is not clear if it is a physical effect or a statistical effect due to the box size we are considering (≈ 12 cMpc)^3.

We have to take into consideration that we are using the Coarse Radiative Transport Approximation (CRTA), ie the radiative flows computations are only executed on the coarsest grid. The dashed line represents $M_{min} = 3.3 \cdot 10^9 M_\odot$, the mass of a halo with a R_{200} of the size of our radiative resolution limit. Halos over this mass are resolved with at least eight flow values. We are aware that the computation of emissivities for halos under this limit can be a bit tricky to interpret, and we will principally focus on halos heavier than M_{min}.

Well resolved halos, with masses over M_{min} are responsible of the major part of the photon budget of our simulations (between 80 and 85 % of photons are coming from theses halos : $\frac{\sum F_{200}(M > M_{min})}{\sum F_{200}} \approx 85\%$), and for those ones the feedback scheme do almost not change the total emissivity at the R_{200} level. We observe in Sec. 4.1 and more particularly on Fig. 4, that the feedback scheme do not change reionization history, we now understand that this is because feedback do not change the halo F_{200} emissivity.

Moreover the order of theses curve is in accordance with the order observed on Fig. 4b ie the F_{200} halo emissivity of the kinetic run is slightly lower than the two other runs, and so its reionization happens last and so on.

If we finally compute the ratio of theses F_{200} halos emissivities and their inner radiative sources (directly linked to the integrated SFR presented in Fig. 7b), we obtain a rough estimation of f_{esc}, the escape fraction of radiative energy. The escape fraction is computed using prescription of (Kimm et al. 2017), ie we consider the time needed by photons to travel from the halo center to R_{200}:

$$f_{esc} = \frac{F_{200}}{\sum \dot{N}_{\left(t - \frac{R_{200}}{c}\right)}}, \quad (14)$$

with $\dot{N}$ the stellar particle emissivity belonging to the current halo. Fig. 9b presents this averaged escape fraction as a function of halo masses.

For radiatively unresolved halos, the observed linearity of the relation is due to a purely numerical effect. For these halos, the flux value became independent of the radius of the computation (as it stays constant within a given cell), and as the halo surface goes with the square of the R_{200} : $\left(S \propto R_{200}^2\right)$ and the halo mass with the third of the R_{200} : $\left(M \propto R_{200}^{1/3}\right)$ it results in a power two third relation between the F_{200} flux and the halo mass: $\left(F_{200} \propto R_{200}^{2/3}\right)$. So we cannot conclude about the escape fraction of radiation for this class of masses.

If we now focus on the well resolved part of the diagram, we observe an increase of the escape fraction for heaviest halos ($M > 10^{10} M_\odot$) for the kinetic feedback scheme.

This explains how the run with kinetic feedback reionize as quickly as other runs, despite its lower SFR: massive halos form less stars but they are more efficient at releasing their photons into the IGM.

The increase of photon escape fraction by supernovae feedback we measure confirm previous works such as eg Kimm & Cen (2014) or Trebitsch et al. (2015). This rise in the escape fraction means that the escaping way of photon is easier, and so that the probability of photon interaction with baryon is lower. If we compare the evolution of the escape fraction to the measured baryon fraction (Fig. 7c), we observe that when baryon fraction is low, the escape fraction tends to be higher and vice versa.

So the change in the halo baryon fraction by super-

novae feedback tends to have a double effect, on one hand it regulates star formation due to a decrease in the available material, but on the other hand this lack of material leads make the photons escape more easy. The unexpected fact is that those two competitive effects almost compensate perfectly with respect to the ionizing photon budget, and so the reionization history seems to be unaffected by the supernovae feedback scheme.

6 CONCLUSION

Even after more than two decades of study, the implementation of supernovae feedback in cosmological simulation is still subject to debate. We present a simple scheme of supernovae energy injection in AMR cosmological simulation code and run a set a simulations varying feedback implementation and model free parameters to show that this scheme is able to regulate star formation on a wide range of halo masses. By computing the R_{200} hydrodynamical velocities of halos, we show that our feedback scheme is able to generate galactic winds and that those winds are linked to the star formation regulation.

Our main results can be summarize as follows.

- Runs with radiation produce a population of low mass ($M < 10^9 M_\odot$) halos with outflowing gas (Fig. 8b). We interpret this population as photo-heated halos, losing their baryons by photo-evaporation.
- The photon budget is mainly governed by massive halos ($M > 10^9 M_\odot$) (Fig. 9a).
- Even with a strong regulation of star formation and thus of the photon budget, the supernovae feedback scheme does not change the reionization history in our simulations, despite a strong impact on the SFR. Indeed, we measure the quantity of radiative energy escaping the R_{200} and show that it does not depend on supernovae feedback (Fig. 9a). We interpret this behavior by considering that the lowering of the baryon fraction, due to the expulsion of baryon by feedback, create easy escape path for the radiation. So, even with a strong regulation of the SFR, and thus of the number of emitted photons, this increase of the escape fraction leads to a comparable number of photons reaching the IGM and thus a similar reionization history.
- The escape fraction of photons of halos with masses over $10^{10} M_\odot$ is increased by a factor ≈ 3 by our kinetic feedback scheme.

This study is based on simulated boxes of modest size (≈ 12 cMpc)^3 so it is not clear if the maximum halo emissivity around $10^{10} M_\odot$ is real or due to a statistical effect. RHD simulations with a bigger simulated volume as CODA (Ocvirk et al. 2015) have been performed and will be used to study this effect. Simulations with better spatial resolution are also planned to address the f_{esc} of low mass halos.

ACKNOWLEDGEMENTS

This work is supported by the ANR ORAGE grant ANR-14-CE33-0016 of the French Agence Nationale de la Recherche.

REFERENCES

Aubert D., Teyssier R., 2008, Monthly Notices of the Royal Astronomical Society, 387, 295
Aubert D., Teyssier R., 2010, ApJ, 724, 244
Aubert D., Deparis N., Ocvirk P., 2015, Monthly Notices of the Royal Astronomical Society, 454, 1012
Bouwens R. J., et al., 2015a, The Astrophysical Journal, 803, 34
Bouwens R. J., Illingworth G. D., Oesch P. A., Caruana J., Holwerda B., Smit R., Wilkins S., 2015b, The Astrophysical Journal, 811, 140
Chardin J., Puchwein E., Haehnelt M. G., 2017, Monthly Notices of the Royal Astronomical Society, 465, 3429
D'Aloisio A., Upton Sanderbeck P. R., McQuinn M., Trac H., Shapiro P. R., 2016, preprint, 1607, arXiv:1607.06467
Dalla Vecchia C., Schaye J., 2012, Monthly Notices of the Royal Astronomical Society, 426, 140
Dubois Y., Teyssier R., 2008, Astronomy and Astrophysics, 477, 79
Fan X., Carilli C. L., Keating B., 2006, Annual Review of Astronomy and Astrophysics, 44, 415
Giallongo E., et al., 2015, Astronomy and Astrophysics, 578, A83
Górski K. M., Hivon E., Banday A. J., Wandelt B. D., Hansen F. K., Reinecke M., Bartelmann M., 2005, ApJ, 622, 759
Haardt F., Madau P., 2012, The Astrophysical Journal, 746, 125
Hahn O., Abel T., 2011, Monthly Notices of the Royal Astronomical Society, 415, 2101
Haiman Z., Rees M. J., Loeb A., 1997, The Astrophysical Journal, 476, 458
Hockney R. W., Eastwood J. W., 1981, Computer Simulation Using Particles
Iliev I. T., Mellema G., Ahn K., Shapiro P. R., Mao Y., Pen U.-L., 2014, Monthly Notices of the Royal Astronomical Society, 439, 725
Katz N., 1992, The Astrophysical Journal, 391, 502
Kennicutt J., 1998, The Astrophysical Journal, 498, 541
Khokhlov A., 1998, Journal of Computational Physics, 143, 519
Kimm T., Cen R., 2014, The Astrophysical Journal, 788, 121
Kimm T., Cen R., Devriendt J., Dubois Y., Slyz A., 2015, arXiv:1501.05655 [astro-ph]
Kimm T., Katz H., Haehnelt M., Rosdahl J., Devriendt J., Slyz A., 2017, Monthly Notices of the Royal Astronomical Society
Leitherer C., et al., 1999, The Astrophysical Journal Supplement Series, 123, 3
Navarro J. F., White S. D. M., 1993, Monthly Notices of the Royal Astronomical Society, 265, 271
Ocvirk P., et al., 2015, preprint, 1511, 11
Planck Collaboration et al., 2015, preprint, 1502, arXiv:1502.01589
Rasera Y., Teyssier R., 2006, Astronomy and Astrophysics, 445, 1
Rosdahl J., Schaye J., Dubois Y., Kimm T., Teyssier R., 2016, preprint, 1609, arXiv:1609.01296
Springel V., Hernquist L., 2003, Monthly Notices of the Royal Astronomical Society, 339, 289
Stinson G., Seth A., Katz N., Wadsley J., Governato F., Quinn T., 2006, Monthly Notices of the Royal Astronomical Society, 373, 1074
Toro E. F., 1997, Riemann solvers and numerical methods for fluid dynamics : a practical introduction. Springer, Berlin, New York, http://opac.inria.fr/record=b1093563
Trebitsch M., Blaizot J., Rosdahl J., 2015. eprint: arXiv:1510.06949, pp 105–108, http://adsabs.harvard.edu/abs/2015sf2a.conf..105T
Veilleux S., Cecil G., Bland-Hawthorn J., 2005, Annual Review of Astronomy and Astrophysics, 43, 769

This paper has been typeset from a TEX/LATEX file prepared by the author.